Available online at www.sciencedirect.com
ScienceDirect
Solid State Sciences 10 (2008) 502–507
Solid State Sciences
www.elsevier.com/locate/ssscie

Thermoelectric properties of $LaCo_{1-x}Ni_xO_3$ polycrystalline samples and epitaxial thin films

Rosa Robert [a], Myriam H. Aguirre [a], Laura Bocher [a], Matthias Trottmann [a], Sebastian Heiroth [b], Thomas Lippert [b], Max Döbeli [c], Anke Weidenkaff [a,*]

[a] *EMPA, Solid State Chemistry and Catalysis, Ueberlandstr. 129, CH-8600 Duebendorf, Switzerland*
[b] *Paul Scherrer Institut, CH-5232 Villigen, Switzerland*
[c] *Ion Beam Physics, Paul Scherrer Institut and ETH Zurich, 8093 Zurich, Switzerland*

Received 15 October 2007; received in revised form 17 January 2008; accepted 21 January 2008
Available online 2 February 2008

Abstract

Epitaxial thin films of $LaCo_{1-x}Ni_xO_3$ were deposited on MgO (100) substrates by pulsed reactive crossed-beam laser ablation (PRCLA). The electrical transport and thermopower of the epitaxial $La(Co,Ni)O_3$ thin films were measured in a broad temperature range and their thermoelectric activity was compared with bulk samples. The measured films show positive Seebeck coefficient values indicative of p-type conduction. The thin films display a better thermoelectric performance at high temperatures compared to the polycrystalline samples.
© 2008 Elsevier Masson SAS. All rights reserved.

Keywords: Thermopower; $LaCoO_3$; Thin films; PLD; Ni-substitution

1. Introduction

The electronic properties of complex cobalt oxides are characterized by the contribution of the 3d orbitals. The interactions of the strongly correlated electrons in these materials are very important and can lead to remarkable physical properties, i.e. magnetoresistance [1], superconductivity, ferroelectricity [2], and thermoelectric activity. The thermoelectric performance of a material is defined by the thermoelectric figure of merit $ZT = S^2/(\kappa \times \rho)$, where S is the Seebeck coefficient or thermopower, ρ the electrical conductivity, and κ the thermal conductivity. Enhanced ZT values are expected for materials with large Seebeck coefficient, low electrical resistivity and low thermal conductivity.

Potential thermoelectric materials are found among the lanthanum cobaltates (e.g. $LaCoO_3$) due to their large Seebeck coefficient of $S \sim 600$ μV/K. It has been shown that the carrier concentration and spin entropy play an important role for the enhancement of the power factor ($PF = S^2/\rho$) in these phases [3,4]. The PF of these materials is tuned by suitable substitutions [5–7]. Previous studies revealed a lowering of the electrical resistivity for low level A- and B-site substituted $LaCoO_3$, e.g. $La_{1-x}Sr_xCoO_3$ [8] and $LaCo_{1-x}Ni_xO_3$ [7,8], while, according to Heikes equation [9–11], the large thermopower of $LaCoO_3$ is preserved.

Recently, a number of structures with low dimensions, such as nano-structured materials, thin films, and superlattices have been proposed to improve the thermoelectric properties of materials. In particular, thin films should exhibit a decrease of the thermal conductivity due to increased phonon scattering, while an increased local electron density of states may improve the thermopower [12]. Intensive research is focused on the evaluation of the thermoelectric properties of complex oxide thin films [13–16]. Epitaxial thin films grown on chemically inert single crystalline substrate materials offer a suitable alternative to large single crystals as ''two-dimensional'' crystals and the possibility to study the influence of the dimensionality on the thermoelectric properties.

* Corresponding author.
E-mail address: anke.weidenkaff@empa.ch (A. Weidenkaff).

1293-2558/$ - see front matter © 2008 Elsevier Masson SAS. All rights reserved.
doi:10.1016/j.solidstatesciences.2008.01.017

This paper reports on the preparation of $LaCo_{0.92}Ni_{0.08}O_3$ thin films grown on MgO (100) substrates by the pulsed reactive crossed-beam laser ablation (PRCLA) technique. The crystallinity, morphology, composition and microstructure of the thin films are characterized in detail. The electric transport and thermopower in these phases are evaluated at 240 K $< T <$ 1000 K. Morphology, composition and crystal structure are related to the measured transport properties. The power factor of the thin film is evaluated and compared to the PF values of polycrystalline samples.

2. Experimental

A soft chemistry synthesis method was applied to prepare a series of powders with a nominal composition of $LaCo_{1-x}Ni_xO_3$ (with $x = 0.05$, 0.08, 0.10) using $La(NO_3)_3 \cdot 6H_2O$ (Merck, >97%), $Co(NO_3)_2 \cdot 6H_2O$ (Merck, >97%), $Ni(NO_3)_2 \cdot 6H_2O$ (Merck, >99%) and citric acid (Sigma–Aldrich) as described in detail in Refs. [17,18]. The resulting polycrystalline phases were pressed into cylinder- and bar-shaped pellets and sintered at $T = 1373$ K.

$LaCo_{0.92}Ni_{0.08}CoO_3$ thin films (LCNO) of different thickness (~86 nm, ~220 nm, and ~395 nm) were grown on MgO (100) substrates by PRCLA. PRCLA is a variation of pulsed laser deposition (PLD) in which a synchronized supersonic gas pulse of a reactive gas intersects the plume [19–22]. The principle of PRCLA is shown in Fig. 1.

The LCNO films were deposited using a KrF excimer laser ($\lambda = 248$ nm, 20 ns pulse width and variable number of pulses) with a laser fluence of 3.0 J/cm^2 and a repetition rate of 10 Hz. The target material was produced from the pressed and sintered $LaCo_{0.92}Ni_{0.08}CoO_3$ powders prepared by the soft chemistry method. The target rod was mounted inside the PLD chamber (see Fig. 1) and was located at 4.0 cm from the substrate. The target material ablated by the KrF laser was deposited on a heated MgO (100) substrate being mounted on a rotatable Mo sample holder at a temperature of $T =$ 823 K. Two oxidizing sources, i.e. oxygen gas to provide a background pressure of $p = 8 \times 10^{-4}$ mbar and a synchronized N_2O gas pulse with a gas pulse duration of 430 μs, were used during the film growth. The pressure in the chamber during the deposition was $p = 10^{-3}$ mbar. The additional oxidizing N_2O source ensures an effective oxidation of the cations due to provision of reactive atomic oxygen species [23]. The time delay between the gas pulse and the laser pulse was 400 μs. At this time delay, the maximum interaction between the ablation plasma and the gas pulse is achieved. The experimental procedure is described in detail in [1,20,23].

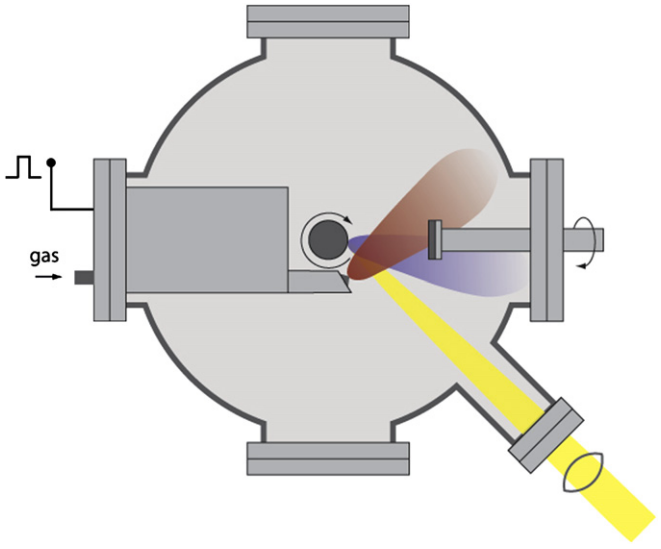

Fig. 1. Scheme of the pulsed reactive crossed-beam laser ablation (PRCLA) setup. A synchronized reactive gas pulse interacts close to the target with the ablation plumes. The ablated species are deposited on rotated heated substrates.

The X-ray diffraction data of the polycrystalline samples were collected by step scanning with a step size of 0.017° over the 2θ range of $20° \leq 2\theta \leq 120°$ on a PANanalytical X'pert diffractometer with Cu K_α radiation. Structural refinements were performed using the FULLPROF program [24]. Structure, crystalline quality and texture of the thin films were studied with a Siemens D5000 X-ray diffractometer with Bragg–Brentano geometry using Cu K_α radiation. The apparatus is equipped with an Eulerian cradle for the sample orientation. The tubular aperture is limiting the beam divergence to 0.3°. Scans in (θ–2θ) geometry under different tilt angles were performed using an aperture of 0.2 mm. X-ray pole figures were measured by rotating the sample around the φ axis and tilting the sample along the χ axis during the measurements with a fixed detector position (2θ).

Experimental Rutherford backscattering spectroscopy (RBS) and particle induced X-ray emission (PIXE) measurements were performed on the thin films using a 2 MeV ^{4}He and 3 MeV proton beam, respectively, with a silicon surface barrier detector at 165° and a Si(Li) X-ray detector under 90° to the incident beam direction. The collected RBS data were analyzed using the RUMP program [25]. In PIXE measurements, the Ni/(Ni + Co) ratio was extracted from the Kα lines after deconvolution of the overlapping Ni K_α and Co K_β signals.

The morphology of the calcined powders and the cross-sections of the sintered pellets were examined by scanning electron microscopy (SEM) using a LEO JSM-6300F.

The thermal conductivity, κ, of the disc-shaped sintered pellets was determined from their density, d, thermal diffusivity, α, and specific heat, c_p using the relationship $\kappa = d \times \alpha \times c_p$. The density was measured by the Archimedes method. The thermal diffusivity (α) was measured using a Netzsch LFA 457 laser flash analyzer in the temperature range of 300 K $< T <$ 1273 K under argon atmosphere. The specific heat was measured using a NETZSCH DSC 404C *Pegasus* differential scanning calorimeter. Electrical transport and Seebeck coefficient measurements were performed using bar-shaped sintered pellets (sintered at $T = 1373$ K in air and dimensions of $5 \times 2 \times 2$ mm^3) and thin films with dimensions of 5–10 mm length and 2–4 mm width. The electrical conductivity and the Seebeck coefficient were determined in the temperature range of 340 K $< T <$ 1240 K using the RZ2001i unit of

Ozawa Science, Japan. Both parameters were recorded simultaneously as a function of temperature in air. The Seebeck coefficient was measured by a steady-state method and the electrical conductivity by the DC four-point method.

3. Results

The diffraction patterns reveal that the $LaCo_{1-x}Ni_xO_3$ (with $0.05 < x < 0.10$) samples do not show secondary impurity phases. The Bragg reflections can be indexed in the rhombohedral structure type with $R\bar{3}c$ S.G. having lattice parameters of $\approx a_p\sqrt{2} \times a_p\sqrt{2} \times 2a_p\sqrt{3}$, $\gamma = 120°$, and atomic positions La (0, 0, 1/4), (Co, Ni) (0, 0, 0) and O (1/2, 0, 1/4) in hexagonal settings [17]. These results are in good agreement with previously reported X-ray [26] and neutron diffraction [27,28] studies on the non-substituted $LaCoO_3$ compound.

The (θ–2θ) scan performed on thin $LaCo_{0.92}Ni_{0.08}O_3$ films grown on MgO substrate reveals the formation of the crystalline perovskite phase. XRD patterns of the films with thicknesses of ~220 nm and ~395 nm show the presence of a La_2O_3 impurity phase, while the LCNO film with a thickness of ~90 nm (LCNO-I in the following) does not contain reflections arising from secondary phases. These results are confirmed by transmission electron microscopic methods. Fig. 2a presents a (θ–2θ) scan for the LCNO at $\chi = 0°$. The LCNO-I thin film crystallizes in the rhombohedral crystal structure ($R\bar{3}c$ S.G.) as the parent $LaCo_{1-x}Ni_xO_3$ polycrystalline material. The X-ray diffractogram contains the $(h00)_{LCNO}$ ($h = 1$, 2, and 3) reflections and the (110) reflection indicative of the perovskite phase indexed in cubic symmetry ($(100)_C \approx (012)_R$), in addition to the (200) reflection of the MgO substrate. The pseudo-cubic a lattice parameter has a value of $a_p = 3.816$ Å which corresponds to $a_H \approx 5.4$ Å.

Fig. 2b shows a (111) pole figure of the LCNO-I film at a fixed $2\theta = 32.86°$. In this figure, four maxima at $\chi = 45.3°$ are visible corresponding to the $(110)_{LCNO}$ reflections, which indicate an in-plane 'cube-on-cube' epitaxy of the LCNO-I film on the MgO (100) substrate. From these results it can be concluded that the LCNO-I film is highly crystalline and grows preferentially along the (100) direction of the MgO.

The a lattice parameter of the MgO single crystal substrate with cubic symmetry has a value of $a = 4.21$ Å. The lattice mismatch α between the substrate and the film along the interface is defined as $\alpha = (a_p\text{substrate} - a_p\text{film})/a_p\text{substrate}$ [1] and corresponds to a value of 9.5%. Thus, a tensile strain appears at the film–substrate interface.

RBS results (see Fig. 3a) reveal that the composition of the LCNO-I film is $La_{1.06\pm0.03}(Co, Ni)O_{2.96\pm0.09}$. From PIXE data analysis, the Ni/(Ni + Co) ratio of 7.7 ± 0.4 at.% is obtained. The LCNO-I film has therefore the same composition as the starting target material. Thus, RBS and PIXE results confirm a congruent ablation of the $LaCo_{0.92}Ni_{0.08}O_3$ phase.

Fig. 3b shows the cross-section SEM image of the LCNO-I thin film. The film thickness measured by a profilometer is around 86 ± 8 nm with a roughness in the range of 0.75 ± 0.06 nm. The film thickness calculated from RBS yields a thickness of 108 ± 3 nm which is slightly higher than for the profilometer traces obtained at the sample edge.

Electric transport and Seebeck coefficient measurements have been used to characterize physical properties of the LCNO-I film. Fig. 4 shows the thermopower of the LCNO-I thin film and LCNO polycrystalline samples. The Seebeck coefficient values of the thin film and polycrystalline samples are positive indicating predominant hole-type carriers in the whole temperature range. The thermopower of both thin film and polycrystalline samples decreases with increasing

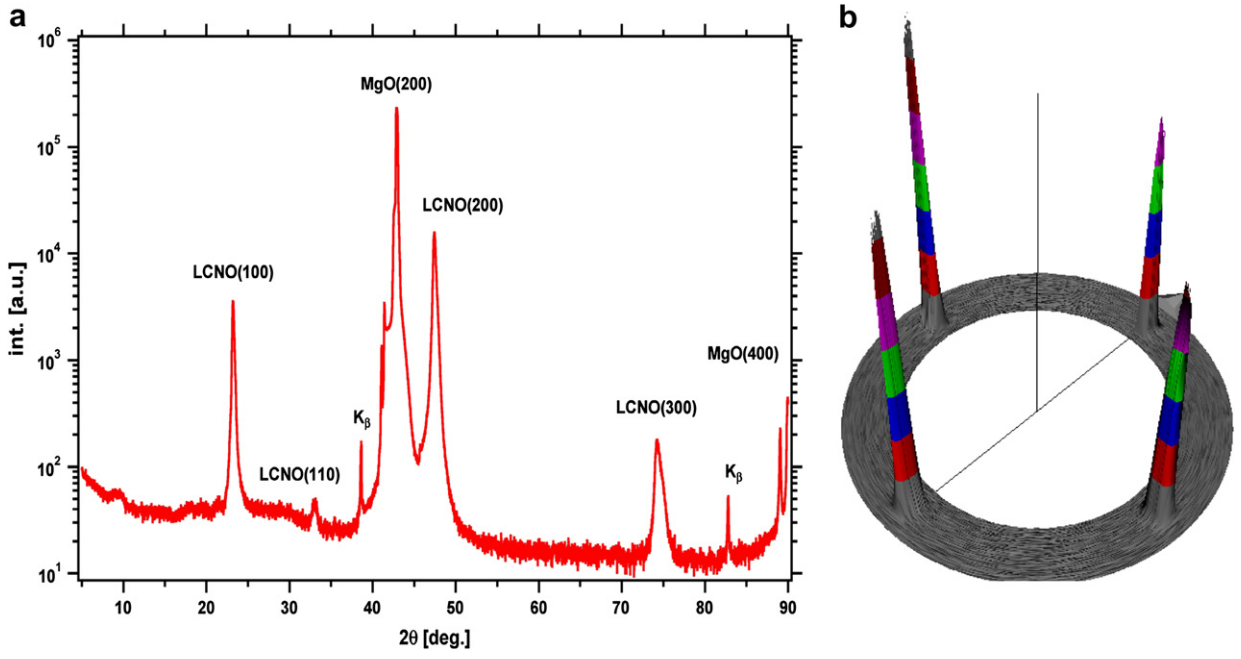

Fig. 2. (a) XRD pattern and (b) pole figure at a fixed $2\theta = 32.86°$ corresponding to the (110) reflection of LCNO-I film grown on MgO substrate.

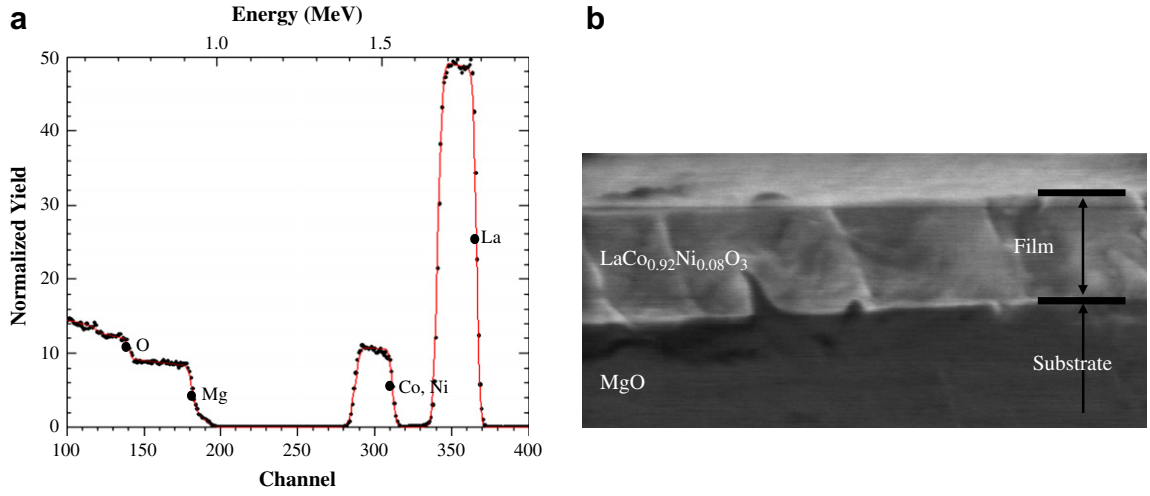

Fig. 3. (a) RBS spectra where the black and red lines represent the experimental and simulated spectrum, respectively and (b) cross-sectional SEM-view of the LCNO-I film grown on MgO.

temperature as expected for the $LaCoO_3$ phases. At $T = 340$ K, the Seebeck coefficient values are $S = +156$ μV/K for the thin film and $S_{(x=0.05)} = +235$ μV/K, $S_{(x=0.08)} = +178$ μV/K, and $S_{(x=0.10)} = +150$ μV/K for the polycrystalline samples, respectively. The experimental Seebeck coefficient data of the polycrystalline samples are well described by Heikes equation [17,30,31], $S = +(k_B/|e|)\ln((1-c_h)/c_h)$, where k_B is the Boltzmann's constant and c_h is the fraction of Co site occupied by a positive charge carrier. The thermopower value of the thin $LaCo_{0.92}Ni_{0.08}O_3$ film is lower than that of $LaCo_{0.92}Ni_{0.08}O_3$ and close to that of $LaCo_{0.90}Ni_{0.10}O_3$ sample. From these results it can be concluded that the thin film possesses a higher concentration of charge carriers compared to the bulk with $x = 0.08$. At $T \sim 700$ K, a crossing of the $S(T)$-curves of both samples, thin film and bulk ($x = 0.08$), is observed and at high temperature the thermopower of the film exceeds the S of the polycrystalline samples with $S_{film} = +17.1$ μV/K and $S_{polycrystalline\text{-}samples} = +8.9-12.7$ μV/K at $T = 1240$ K.

Fig. 5a displays the electrical resistivity of the thin film and polycrystalline samples. The substitution of Co by Ni ions in the cobaltate structure induces a decrease of the electrical resistivity compared to that of the non-substituted $LaCoO_3$ [31]. The decrease in the electrical resistivity is associated with an increase in Co^{4+} content and charge carriers in the system. The Co^{4+} formation is induced by the substitution of the Co^{3+} by Ni^{2+} ions [8,31]. All samples, bulk and thin film, exhibit the same tendency: the electrical resistivity decreases with increasing temperature ($d\rho/dT < 0$), representing a semiconductor-type behaviour in the temperature range of $340\ K < T < 800\ K$. The thin film exhibits an electrical resistivity value of $\rho = 135$ mΩ cm at $T = 340$ K which is higher than the value of the polycrystalline sample ($x = 0.08$) of $\rho = 60$ mΩ cm. Above $T = 800$ K, the polycrystalline samples

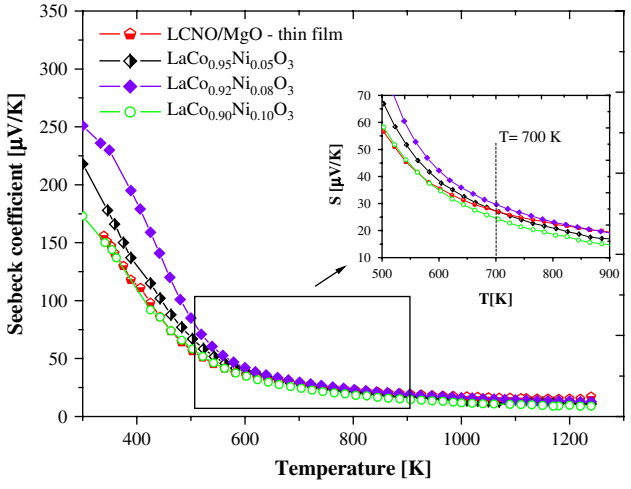

Fig. 4. Seebeck coefficient measurements of thin $LaCo_{0.92}Ni_{0.08}O_3$ film and polycrystalline $LaCo_{1-x}Ni_xO_3$ ($x = 0.05$, 0.08, and 0.10) in the temperature range of $340\ K \leq T \leq 1240$ K.

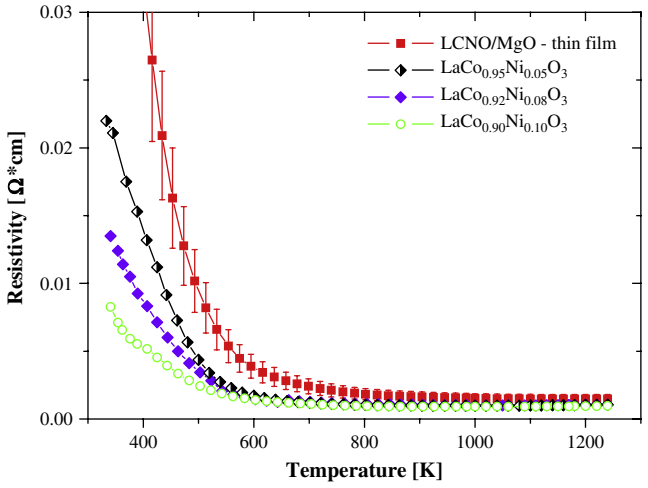

Fig. 5. Electrical resistivity measurements of LCNO-I thin film- and polycrystalline-samples in the temperature range of $340\ K \leq T \leq 1240$ K.

and the thin film show a low electrical resistivity of $\rho = 0.96-1.05\ \mathrm{m\Omega\,cm}$ and $\rho = 1.31\ \mathrm{m\Omega\,cm}$, respectively.

A lower electrical resistivity compared to the bulk is expected for the epitaxial LCNO film, since in the polycrystalline material the electrical resistivity is generally affected by the grain boundaries. Nevertheless, it should be pointed out that the electrical resistivity of the polycrystalline La(Co, Ni)O_3 phases shows similar values compared to the electrical resistivity reported for single crystals [8].

In a previous study, it has been shown that a $La_{1-x}Ca_xMnO_{3-\delta}$ thin film of 210 nm thickness exhibited a lower electrical resistivity compared to the parent bulk compound [29]. However, in thin films with low thickness, the electrical transport can be affected by the strain originated from the film–substrate interface [1]. Several studies about the effect of the film thickness on transport properties showed an increase of the electrical resistivity for a decreasing film thickness [32,33]. Therefore, it can be considered that the increased electrical resistivity observed in the epitaxial thin film compared to the polycrystalline samples might be related to the low thickness of the film (th = 86 nm), but further studies are needed to confirm this point.

The LCNO-I thin film exhibits a power factor lower than the parent bulk compound close to room temperature which is mainly due to its higher resistivity. Nevertheless, the highest PF at high temperature ($T = 1220$ K) belongs to the LCNO-I thin film and has a value of $\mathrm{PF} = 2.17 \times 10^{-5}\ \mathrm{W/K^2\,m}$, which is twice the value of the polycrystalline LCNO-I sample ($\mathrm{PF} = 1.12 \times 10^{-5}\ \mathrm{W/K^2\,m}$). The thin film exhibits a higher value of electrical resistivity and a comparable value of the thermoelectric power with respect to the polycrystalline sample at room temperature. The $\rho(T)$-curves for both materials present a similar behaviour in the whole measured temperature range. However, the $S(T)$-curves present an intersection at $T = 700$ K. As a result, the thin film shows higher thermoelectric performance at high temperatures.

A ZT value in the range of ZT ~ 0.01 at 1220 K is estimated for the thin film sample using the PF value of the thin film obtained at $T = 1220$ K and the thermal conductivity value of the polycrystalline $LaCo_{0.95}Ni_{0.05}O_3$ phase $\kappa_{(T=1220\ \mathrm{K})} = 2.4\ \mathrm{W/m\,K}$. The ZT values for the polycrystalline samples are around ZT ~ 0.006 at 1220 K.

4. Conclusions

The polycrystalline cobaltate phases with the composition $LaCo_{1-x}Ni_xO_3$ (with $x = 0.05$, 0.08, and 0.10) crystallize in the rhombohedral structure type with $R\bar{3}c$ S.G. Thin $LaCo_{0.92}Ni_{0.08}O_3$ films have successfully been deposited on MgO substrates by PRCLA keeping the target composition. The LCNO-I thin film is highly crystalline and grows preferentially along the (100) direction of the MgO substrate. The evolution of the thermopower values upon nickel substitution in these phases is well described by Heikes equation. In thin films, the electrical transport might be affected by the strain originating from film–substrate interface.

Above a temperature of $T \sim 700$ K, the Seebeck coefficient of the thin film exhibits a higher value compared to the Seebeck coefficient of the polycrystalline sample. The single crystalline $LaCo_{0.92}Ni_{0.08}O_3$ thin film exhibits a higher electrical resistivity and a similar thermoelectric power compared with the polycrystalline sample. On the contrary, the electrical transport might be affected by the strain in the film–substrate interface. The thin film displays better thermoelectric performance at high temperatures.

Acknowledgements

Financial support by the Swiss Federal Office of Energy, EMPA and the Paul Scherrer Institut is gratefully acknowledged.

References

[1] S. Canulescu, T. Lippert, H. Grimmer, A. Wokaun, R. Robert, D. Logvinovich, A. Weidenkaff, M. Döbeli, Appl. Surf. Sci. 252 (2006) 4599.
[2] B. Raveau, Prog. Solid State Chem. 35 (2007) 171.
[3] W. Koshibae, K. Tsutsui, S. Maekawa, Phys. Rev. B 62 (2000) 6869.
[4] W. Koshibae, S. Maekawa, Phys. Rev. Lett. 87 (2001) 236603.
[5] A. Maignan, D. Flahaut, S. Hébert, Eur. Phys. J. B 39 (2004) 145.
[6] S. Hébert, D. Flahaut, C. Martin, S. Lemonnier, J. Noudem, C. Goupil, A. Maignan, Prog. Solid State Chem. 35 (2007) 457.
[7] R. Robert, L. Bocher, M. Trottmann, A. Reller, A. Weidenkaff, J. Solid State Chem. 179 (2006) 3867.
[8] Y. Kobayashi, S. Murata, K. Asai, J.M. Tranquada, G. Shirane, K. Kohn, J. Phys. Soc. Jpn. 68 (1999) 1011.
[9] R.R. Heikes, R. Mazelsky, R.C. Miller, Physica 30 (8) (1964) 1600.
[10] N. Tsuda, K. Nasu, A. Fujimori, K. Siratori, Electronic Conduction in Oxides, Springer, 2000.
[11] J.-S. Zhou, J.B. Goodenough, Phys. Rev. B 60 (1999) R15002.
[12] L.D. Hicks, M.S. Dresselhaus, Phys. Rev. B 47 (1997) 16631.
[13] T. Terada, Y. Yoshida, M. Ueno, Y. Takai, J. Ceram. Soc. Jpn. 110 (2002) 560.
[14] J.G. Moyer, D.A. Kukuruznyak, N. Nguyen, M.S. Prowse, F.S. Ohuchi, J. Appl. Phys. 100 (2006) 083504.
[15] H.W. Eng, W. Prellier, S. Hébert, D. Grebille, L. Mechin, B. Mercey, J. Appl. Phys. 97 (2005) 013706.
[16] A. Sakai, T. Kanno, S. Yotsuhashi, S. Okada, H. Adachi, J. Appl. Phys. 99 (2006) 093704.
[17] R. Robert, L. Bocher, B. Sipos, M. Döbeli, A. Weidenkaff, Prog. Solid State Chem. 35 (2007) 447.
[18] M.H. Aguirre, R. Robert, D. Logvinovich, A. Weidenkaff, Inorg. Chem. 46 (2007) 2744.
[19] M.J. Montenegro, M. Döbeli, T. Lippert, S. Müller, B. Schnyder, A. Weidenkaff, P.R. Willmott, A. Wokaun, Phys. Chem. Chem. Phys. 4 (2002) 2799.
[20] M.J. Montenegro, T. Lippert, S. Müller, A. Weidenkaff, P.R. Willmott, A. Wokaun, Appl. Surf. Sci. 197 (2002) 505.
[21] M.J. Montenegro, C. Clerc, T. Lippert, S. Müller, P.R. Willmott, A. Weidenkaff, A. Wokaun, Appl. Surf. Sci. 208 (2003) 45.
[22] T. Lippert, M.J. Montenegro, M. Dobeli, A. Weidenkaff, S. Muller, P.R. Willmott, A. Wokaun, Prog. Solid State Chem. 35 (2007) 221.
[23] S. Canulescu, T. Lippert, A. Wokaun, R. Robert, D. Logvinovich, A. Weidenkaff, M. Döbeli, M. Schneider, Prog. Solid State Chem. 35 (2007) 241.
[24] J. Rodríguez-Carvajal, In: Satellite Meeting of the XVth Congress of the International Union of Crystallography, Toulouse, France.
[25] L.R. Doolittle, Nucl. Instr. Meth. B 15 (1986) 227.
[26] P.M. Raccah, J.B. Goodenough, Phys. Rev. B 155 (1967) 932.

[27] G. Thornton, B.C. Tofield, A.W. Hewat, J. Solid State Chem. 61 (1986) 301.
[28] P.G. Radaelli, S.-W. Cheong, Phys. Rev. B 66 (2002) 094408.
[29] M.H. Aguirre, S. Canulescu, R. Robert, N. Homazava, D. Logvinovich, L. Bocher, T. Canulescu, A. Weidenkaff, J. Appl. Phys. 103 (2008) 013703.
[30] R. Robert, M.H. Aguirre, P. Hug, A. Reller, A. Weidenkaff, Acta Mater. 55 (2007) 4965.
[31] R. Robert, L. Bocher, M. Trottmann, A. Reller, A. Weidenkaff, J. Solid State Chem. 179 (2006) 3893.
[32] G. Herranz, B. Martínez, J. Fontcuberta, F. Sánchez, C. Ferrater, M.V. García-Cuenca, M. Varela, Phys. Rev. B: Condens. Matter 67 (2003) 174423.
[33] M. Bibes, L. Balcells, S. Valencia, S. Sena, B. Martínez, J. Fontcuberta, S. Nadolski, M. Wojcik, E. Jedryka, J. Appl. Phys. 89 (2001) 6686.